

https://dspace.org/

Experimental analysis and numeracal simulation of biomass pyrolysis

Yasser Elhenawy; K Fouad; M Bassyouni; M Gadalla; F Ashour ...

SPRINGER
https://hdl.handle.net/10539/43444
WOS

Downloaded from a DSpace repository. https://dspace.org/

Journal of Thermal Analysis and Calorimetry (2024) 149:10369–10383
https://doi.org/10.1007/s10973-024-12987-y

Experimental analysis and numerical simulation of biomass pyrolysis

Yasser Elhenawy[1,2] · Kareem Fouad[3] · Amr Mansi[4,5] · M. Bassyouni[4,5,7] · Mamdouh Gadalla[4] · Fatma Ashour[6] · Thokozani Majozi[1]

Received: 4 July 2023 / Accepted: 31 January 2024 / Published online: 12 April 2024
© The Author(s) 2024

Abstract
Finding alternatives to fossil fuels is extremely important for economic and environmental considerations. Biomass pyrolysis stands out as an efficient method for generating fuels and chemical intermediates. This study explored the influence of wood particle size (ranging from 1 to 3 cm) and pyrolysis temperature (ranging from about 300 to 480 °C) on the process. Characterization of wood residues utilized energy-dispersive X-ray (EDX) and field emission scanning electron microscopy (FE-SEM) to comprehend surface morphology and resultant biochar structure. Results revealed a significant temperature-dependent impact on pyrolysis product concentrations. Biomass composition analysis indicates lignin, hemicellulose, extractive contents, and cellulose percentages at 11.23%, 39%, 2.15%, and 47.62% mass/mass, respectively. Reduction in particle size to less than 2 mm enhances heat transfer, elevating overall bio-oil production. Major bio-oil components comprise phenolics, acids, alcohols, aldehydes, and ketones. Optimal conditions are identified at a wood particle size of 1 cm and a heating temperature of 480 °C. For every 1.0 kg of wood biomass residues, bio-oil, syngas, and biochar yields are 0.38 kg, 0.22 kg, and 0.4 kg, respectively. Notably, the agreement between Aspen Plus simulation and experimental findings underscored the robustness of the study.

Keywords Biomass pyrolysis · Characterization · Biofuels · Simulation

Introduction

Crude petroleum fuels offered only 4% of the world's energy requirements at the beginning of the twentieth century. However, at present petroleum fuels are considered the most vital energy source, covering 40% of global energy consumption. It also provides 96% of all transportation fuels [1–5].

However, the combustion of fossil fuels emits carbon dioxide (CO_2) and other greenhouse gases (GHGs), which trap heat in the atmosphere and become the primary cause of global warming and climate change. According to statistics, global CO_2 emissions from fuel burning were 32.31 Gt of CO_2 in 2016, with an increase of 40% since 2000.

✉ Yasser Elhenawy
dr_yasser@eng.psu.edu.eg

✉ Thokozani Majozi
thokozani.majozi@wits.ac.za

Kareem Fouad
engkareem.s.civil@gmail.com

Amr Mansi
amrmansi24@gmail.com

M. Bassyouni
m.bassyouni@eng.psu.edu.eg

Mamdouh Gadalla
mamdouh.gadalla@yahoo.com

Fatma Ashour
fhashour@yahoo.com

[1] School of Chemical and Metallurgical Engineering, University of the Witwatersrand, 1 Jan Smuts Avenue, Johannesburg 2000, South Africa

[2] Department of Mechanical Power Engineering, Faculty of Engineering, Port Said University, Port Said 42526, Egypt

[3] Civil Engineering Department, Higher Future Institute of Engineering and Technology, El Mansoura, Egypt

[4] Department of Chemical Engineering, Faculty of Engineering, Port Said University, Port Said 42526, Egypt

[5] Center of Excellence for Membrane Testing and Characterization (CEMTC), Port Said University, Port Said 42526, Egypt

[6] Department of Chemical Engineering, Cairo University, Giza 12613, Egypt

[7] East Port Said University of Technology, Sinai, Port Said 45632, Egypt

Furthermore, GHGs affect living organisms, particularly the human respiratory system. As a result, there is a growing interest in environmentally friendly and sustainable energy sources [6–9]. The energy crisis has escalated worldwide due to global population increase, growing energy needs, and the continuous depletion of fossil-based fuel reserves [10–12].

Annually, significant amounts of agro-industrial, municipal, and forestry residues are managed as waste; however, they can be recycled and reused to generate thermal and electrical energy using biological or thermo-chemical conversion processes. The most promising approaches for generating energy from various wastes are solid fuel pyrolysis and gasification [13–17]. The use of biomass fuels for energy production can help to reduce greenhouse gas emissions and other pollutants, which is crucial for achieving the recent emission limit [18]. The raw material is heated to elevated temperatures in an oxygen-free atmosphere during the pyrolysis process, resulting in char and condensable (tar) and non-condensable gaseous fractions. The primary purpose of the pyrolysis process is to convert as much of the input material as feasible. The procedure is frequently undertaken to obtain the best feasible yield of a given fraction [19, 20].

Biomass is a renewable energy source that is widely available around the world. Sustainable biomass energy usage is an alternative for partially replacing the use of fossil fuels and nuclear energy. Rural populations in developing countries, which represent over half of the world's population, rely on biomass energy [21, 22]. Waste biomass generally requires further treatment, such as thermochemical conversion, to enhance its energy characteristics to meet the requirement for direct burning due to its low energy density and high moisture and contaminant content [18, 23]. To evaluate the impact of slow pyrolysis process parameters on rice husk biochar output, a fixed bed reactor was utilized. For this reason, Taguchi's approach (L9) was applied, whereby four variables were adjusted by three distinct levels: temperature (T) of 300, 400, and 500 °C; residence duration (t) of 3600, 5400, and 7200 s; rice husk mass (m) of 125, 250, and 500 g; heating rate (β) of 5, 10, and 20 °C min^{-1}. The results show that 400 °C, 10 °C min^{-1} heating rate, 3600 s residence time, and 500 g of biomass (Test 5) are the ideal operating conditions for the slow pyrolysis procedure to be efficient and thermally viable. This is because a significant amount of biochar yield (187.55 g) with notable thermal properties (HHV = 21.53 MJ/kg, FC = 45.89 and C = 52.13) and low energy consumption (1200 kWh) was achieved [24].

It has been investigated whether lignin may be converted into phenols using carbon materials generated through biomass pyrolysis. Employing guaiacol as an instance molecule, the control process of free radicals on the specificity of phenolic compounds was explored. The findings demonstrated that alternative processes might be used by gaseous radicals or carbon-centered radicals of carbon materials to induce the synthesis of phenols. Methyl radicals primarily regulated the selectivity of phenols in gas-phase systems, resulting in a theoretical selectivity of phenols less than 50%. Methyl and phenolic radicals were quickly and readily deposited on the carbon border sites in the heterogeneous solution. The crucial intermediate, the o-hydroxyphenoxy radical, was initially absorbed on the carbon center radical sites, where phenols were generated at the same location following desorption and hydrogenation [25]. For studying the thermochemical reaction mechanism and optimizing the pyrolysis process, modeling and simulation are favorable approaches. Modeling and simulation studies save both the time and cost required for practical investigations. Aspen Plus is a sophisticated system-oriented process engineering software that allows for the modeling of physical, chemical, and biological processes [26].

Various modeling techniques for modeling of biomass pyrolysis were used in the literature including Aspen Plus, artificial neural network, and computational fluid dynamics. However, Aspen Plus has gained a widespread popularity because it avoids the use of intricate reaction mechanisms, provides a simple modeling approach that contains the primary pyrolysis reactions, and contains extensive components and properties libraries. Aspen Plus is extensively used to develop multiple biomass models to calculate mass and energy balance on units, as well as monitor and optimize process performance, thanks to its sophisticated algorithms and comprehensive database [27, 28]. Several recent studies have presented the simulation of the pyrolysis process. For example, Aspen Plus software was utilized as modeling software, while rice straw and sugarcane bagasse were chosen as biomass raw materials. The simulated biochar yield value differs from the experimental value. The difference is minimal at low temperatures (300–500 °C) and relatively considerable at high temperatures (600–800 °C), although both stay within the range of 0.55–8.93% [29]. Another study has evaluated a developed steady-state model using the Aspen Plus simulation program to forecast the pyrolysis product yields of fruit wastes. The model was run with the specifics of the proximate and elemental analyses of the fruit wastes as input parameters, and the simulation was run at 300–600 °C and 1 atm pressure. Date pits had the highest char yield (50.92 mass%) among the fruit wastes, whereas mango endocarp had the highest syngas output (54.23 mass%). According to the simulation findings, date pits are most suitable for biochar synthesis, while mango endocarp and orange peel are best suited for syngas production [30]. Using Aspen Plus software, another study has simulated a four-stage steady-state model for the pyrolysis procedure performance simulation. The moisture content of the municipal green waste (MGW) feed is reduced in the first

step. In the second step, the MGW is divided into its basic elements. The condensate substance is separated in the third stage, and the pyrolysis reactions are finally modeled using the Gibbs free energy minimization methodology. The ultimate and proximate analyses' results from the MGW were used as input parameters in the Aspen Plus simulation. The model is validated using experimental data. The variance between the MGW's modeling and experimental elemental compositions was revealed to be 7.04% for nitrogen, 7.3% for carbon, 15.82% for hydrogen, and 5.56% for sulfur [31].

While numerous studies have investigated sawdust pyrolysis [32.33], there is a distinct scarcity of research exploring the impact of operational parameters, such as temperature and particle size, at the pilot scale and its correlation with simulation outcomes. This study addressed this gap, introducing a novel perspective by systematically investigating these crucial factors and their interplay, thereby contributing valuable insights to the existing body of knowledge.

Materials and methods

Feedstock

The raw material employed in this investigation is wood residues, provided by a furniture workshop located in Port Said region, Egypt. The particle sizes for the collected wood ranged between 1 and 3 cm. The ultimate and proximate examination of feedstock segments was conducted with an automatic proximate analyzer (SDTGA5000, Sundy, China) and an elemental analyzer (VarioEL III, Germany), respectively. The concentration of biomass was determined using the mass differential. An IKA C200 bomb calorimeter oxygen bomb calorimeter is used to determine the calorific value of wood residues. The wood FESEM and EDX analyses were performed with field emission scanning electron microscopy (FE-SEM; Schottky-JSM-7610F), Japan. Fourier transform infrared spectroscopy (BRUKER ALPHA II FTIR) was utilized to detect the functional groups present in the biochar produced at three different particle sizes.

Pyrolysis reactor explanation and process

In the present study, wood residues were continuously pyrolyzed in a pyrolysis reactor. The proposed pyrolysis process schematic diagram is given in Fig. 1. Investigations were carried out by altering the pyrolysis temperatures between 290 and 480° C in the presence of nitrogen. The proposed heating rates were according to a previous GC–MS investigation where there is significant fragmentation of the sawdust as recommended in the previous literature [34, 35]. The measurements were carried out at a heating rate of 10 °C min^{-1} and for 15 min. The PLC was utilized to control the heating rate, target temperature, and holding duration of the torrefaction to achieve the desired output. For each operation, a tubular reactor containing 1.0 kg of air-dried wood residues was used. Liquefied petroleum gas (LPG) was utilized as a heating energy source for feedstock to reach the desired temperature in the reactor. The pyrolysis reactor is constructed of an iron sheet tube 650 mm in length and 400 mm in diameter, as shown in Fig. 2a and b. Organic vapors were collected at a temperature of 20 °C using a heat exchanger from a type (flat plate) condensing machine. On opposing ends, the tube has a sealed end and a flange. The syngas was obtained from the reactor end and carried into the condensing unit to separate the condensable and non-condensable gases. A detailed description of the reactor and condenser is presented in Table 1.

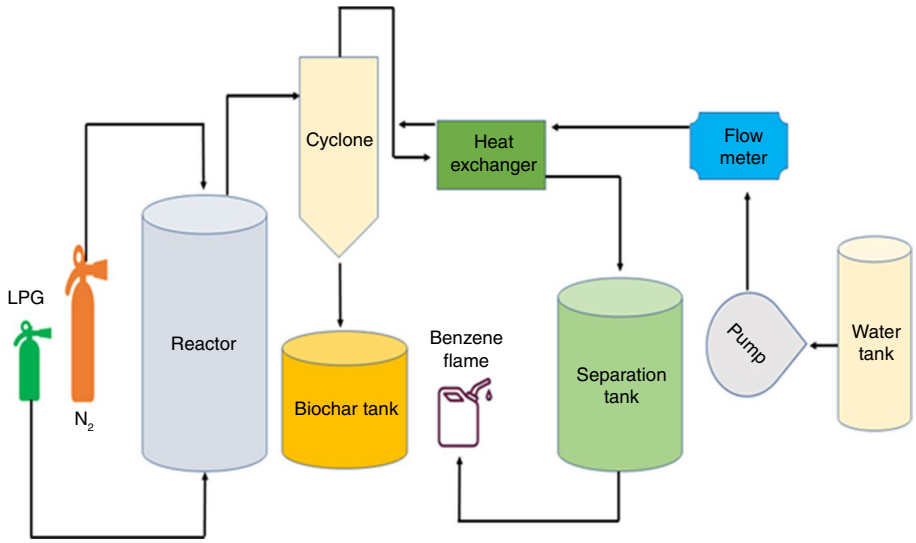
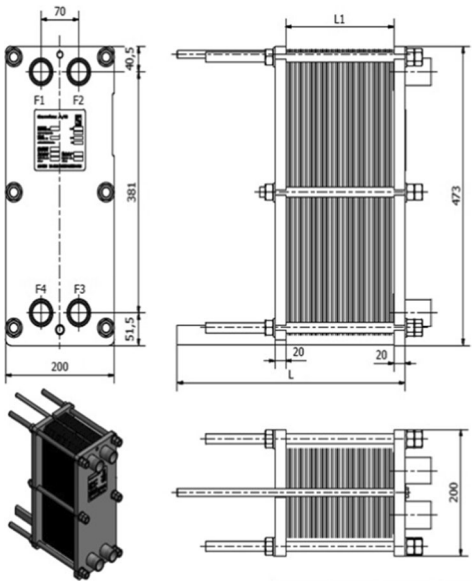
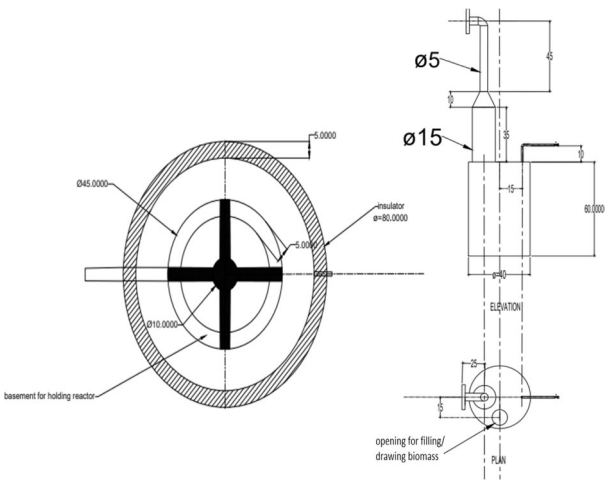


Fig. 1 Flow diagram of the pyrolysis system utilized in this study



Fig. 2 **a** Actual pyrolysis system utilized in the study, **b** pyrolysis reactor. 1. LPG cylinder. 2. Nitrogen cylinder. 3. Furnace. 4. Reactor. 5. Cyclone separation. 6. Heat exchanger. 7. Fuel storage tank. 8.Water Tank. 9. Water pump. 10. Burner

Table 1 Specifications of the main units of the pyrolysis system

Bio-gas plate frame condenser specifications	
Number of plates: 14 Active heat transfer area: 0.6 m^2 Design duty: 11 kW Material of construction: titanium	
Pyrolysis reactor specifications	
Reactor capacity: 74 L Material of construction: galvanized steel Insulation material: rock wool	

A 1.0-liter tubular glass container was utilized to accumulate the final formed bio-oil before assessing its chemical elemental components. A gas analyzer was employed to measure the output syngas components. Furthermore, the yield was determined by removing the biochar from the apparatus and weighing it. By using equations (Eqs. (1–3)), the yield of final products was determined as follows:

$$\text{Bio}-\text{oil yield}(\%) = \frac{\text{Mass of Bio}-\text{oil}}{\text{Mass of Biomass}} \times 100 \tag{1}$$

$$\text{Biochar yield}(\%) = \frac{\text{Mass of Biochar}}{\text{Mass of Biomass}} \times 100 \tag{2}$$

$$\text{Masslosses}(\%) = \left[100 - (\text{biocharyield}\% + \text{bio} - \text{oilyield}\% + \text{gasyield}\%)\right] \tag{3}$$

Simulation study of slow pyrolysis using Aspen Plus

The simulation of wood residues was carried out by the Aspen® Plus V.11 software. The property method used in the simulation study is Redlich–Kwong–Soave with Boston–Mathias alpha function because it is highly suitable for the modeling of synthetic fuels [36]. MIXCINC was set as the global stream class of the simulation. The specific property methods for density and enthalpy were chosen as DGOALIGT and HCOALGEN, respectively. The proximate and ultimate analyses of the wood samples are required for the simulation of the pyrolysis process. Both analyses were measured experimentally. Biochar is formed in the actual pyrolysis reactor. Bio-oil is formed and simulated as a pseudo-component having an average molar mass and boiling point that resembles the mixtures of components revealed by the GC mass analysis. The average molar mass and average boiling point of the bio-oil were calculated by using the formulas in (Eqs. 4 and 5) by making use of the concentration profile generated by the GC mass analysis of the bio-oil.

$$M_{\text{w avg}} = \sum_{i=1}^{n} M_{\text{wi}} x_{\text{i}} \tag{4}$$

$$T_{\text{b avg}} = \sum_{i=1}^{n} T_{\text{bi}} x_{\text{i}} \tag{5}$$

where M_{wi} is the molar mass of any species i and T_{bi} is the boiling point of any species i. Biogas is simulated to have the same elements that were detected experimentally (i.e., CO, CO_2, H_2, CH_4, and H_2O). The RGIBBS (Gibbs) reactor was utilized for the modeling of the pyrolysis process. The RGIBBS block in Aspen Plus cannot identify the biomass by its proximate and ultimate analyses. Therefore, the biomass was modeled by introducing its basic monomers that constitute cellulose, hemicellulose, and lignin. Cellulose and hemicellulose were represented in the simulation by the monomers xylose ($C_6H_{10}O_5$). Lignin was represented by three different monomers, namely p-coumaryl alcohol, sinapyl alcohol, and coniferyl alcohol. The coniferyl alcohol and p-coumaryl monomers were not available in the Aspen Plus database, and their structural formula and properties were added manually into the software. The monomers have different H/C and O/C ratios which permits adjusting the fractions of the monomer present to the biomass composition. The nitrogen content of the biomass was represented by two nitrogen-containing organic monomers, namely glutamic acid and pyrrole. The amino acid represents the proteins in the biomass while pyrrole is the basic compound of a more complex amino acids and naturally occurring pigments such as porphyrins and chlorophyll [37]. The principles of the Gibbs reactor are based on Gibbs free energy minimization approach. At constant temperature and pressure, a chemical reactions proceeds until the composition within the reactor has the lowest possible Gibbs free energy. This is represented mathematically as follows (Eq. 6):

$$\mathrm{d}G = \left(\frac{\mathrm{d}G}{\mathrm{d}T}\right)_{\text{P,N}} \mathrm{d}T + \left(\frac{\mathrm{d}G}{\mathrm{d}P}\right)_{\text{T,N}} \mathrm{d}P + \sum_{i=1}^{n} \left(\frac{\mathrm{d}G}{\mathrm{d}N_{\text{j}}}\right)_{\text{T,P,N}_{\text{i}}} \mathrm{d}N_{\text{j}} \tag{6}$$

At constant temperature and pressure, Eq. 6 reduces to:

$$\mathrm{d}G = \sum_{i=1}^{n} \left(\frac{\mathrm{d}G}{\mathrm{d}N_{\text{j}}}\right)_{\text{T,P,N}_{\text{i}}} \mathrm{d}N_{\text{j}} = \sum_{i=1}^{n} \mu_{\text{j}} \mathrm{d}N_{\text{j}} \tag{7}$$

where dG is the change in Gibbs free energy, T is the system temperature, P is the system pressure, N_{i} is the number of moles of a specific component i, and μ is the chemical potential.

The conversion of biomass to its basic components was done by rigorous spreadsheet calculations. The simulation of the process is shown in Fig. 3. The system comprised the pyrolysis reactor, solids separator modeled by the SSPLIT block, vapors condenser modeled by the HEATER block, and the liquid–vapor flash vessel modeled by the FLASH2 block. The temperature varied in the simulation from 290 to 480 °C with a 10 °C interval. The biochar, bio-oil, and pyrolytic gas yields are compared with the experimental results.

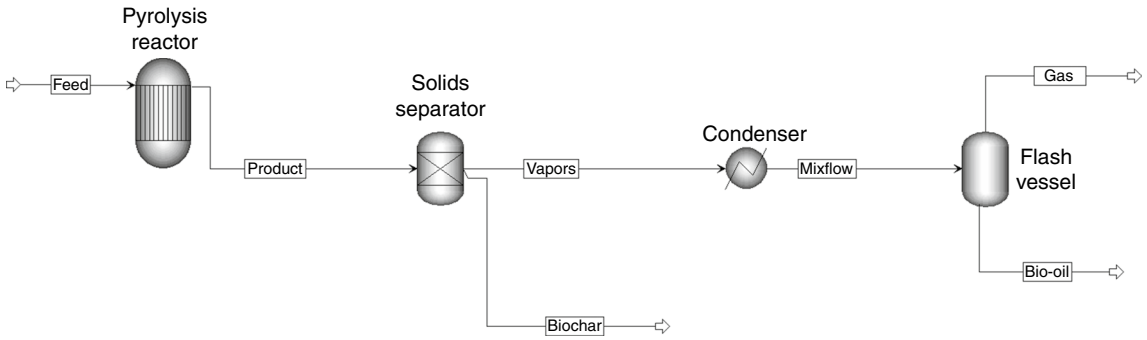


Fig. 3 Simulation of the pyrolysis of wood using Aspen Plus software

Result and discussion

Characteristics of biomass

Different characteristics of wood residues and biochar, the outcomes of proximate and ultimate analyses, as well as the atomic ratios of H/C, O/C, and HHV of biochar are listed in Table 2. The moisture content for sawdust and biochar was 3.07% and 1.12%, respectively. The moisture content of the biomass was noticed to be less than 10%. Also, wood residues showed a well thermochemical transformation due to their high volatile content (80.87%) and low ash content (3.38%) which produces biochar with high fixed carbon content and better heating value. These findings show the superiority of wood residues as a feedstock in the pyrolysis process. Fixed carbon content in wood residues reached 12.68% with higher amounts of O and C rather than N and H. During the pyrolysis process, the increase in oxygen quantity in the biomass resulted in oxygenated liquid outputs. However, lower sulfur and nitrogen content in the feedstock biomass is desired due to fewer SOx and NOx releases during the decomposition process. The empirical elemental formula for the biomass is $CH_{1.83}O_{0.75}N_{0.009}$ using the elemental composition data. O/C and H/C lower ratios show superior energy substances.

These results indicate that the proposed wood residues exhibit a suitable feedstock for pyrolysis. The lignin, hemicellulose, extractive contents, and cellulose percentages in the biomass are 11.23, 39, 2.15, and 47.62, respectively.

Effect of the operating parameters on the product yield

Effect of temperature

The concentration of the final pyrolysis products (biochar, pyrolytic gas, and bio-oil) is significantly influenced by temperature. Liquid oil is produced through the pyrolysis of biomass because the lignocellulosic portion of the biomass matter is instantly decomposed and depolymerized [38]. The particle size for the wood residues in the experimental study ranged from 1 to 3 cm. The bio-oil yield showed a significant increase with the reduction in the particle size and reached its maximum value at a particle size of 1 cm as illustrated in Fig. 4a. Moreover, the yield reached the maximum of 38% at a pyrolysis temperature of 480 °C. Also, increasing the pyrolysis temperature from 290 to 480 °C has significantly raised the bio-oil yield from 2 to 38%. The improvement in bio-oil yield is due to the enhanced breaking of the chemical bonds within the biomass fragments [39]. In contrast, with increasing pyrolysis temperature from 290 to 480 °C the char yield decreased from 92 to 45% for particle size of 1 cm as shown in Fig. 4b. The greater breakdown of lignin in biomass materials is a major factor in a reduction in char output at higher temperatures [40]. Usually, lower particle sizes become heated and blown away rapidly due to easy heat transfer [41]. With rising heating temperatures, the yield of syngas constantly grows. As shown in Fig. 4c, when the temperature rises from 290 to 480°C, the gas yield increases from 2 mass% to 32 mass% for a particle size of 1 cm. Enhanced biomass conversion can explain why gas output rises as temperatures rise [42].

Table 2 Characterization of wood residue feedstock

Raw material	Proximate analysis / mass%^{ad}				Ultimate analysis / mass%				HHV / MJ kg^{-1}	H/C Molar proportion	O/C Molar proportion
	Moisture	Ash	Fixed carbon	Volatile matter	N	O^{a}	H	C			
Wood residue	3.07	3.38	12.68	80.87	0.50	46.39	7.02	46.09	18.67	1.83	0.75
Biochar	1.12	11.86	65.63	21.57	0.72	32.94	2.86	63.48	22.03	0.54	0.38

Effect of particle size

Particle size influence on the biofuel yield is illustrated in Fig. 5. For particle size of 1 cm as shown in Fig. 5a, the results show a superior conversion for the biomass residues. At 480 °C, the product yields were 38, 22, and 40 mass% for bio-oil, syngas, and biochar, respectively. By increasing particle size to 2 cm as shown in Fig. 5b, the biofuel yield at 480 °C has shown 26% and 18 mass% for bio-oil and syngas, respectively. The decrease in bio-oil and syngas productivity has continued with increasing particle size to 3 cm as shown in Fig. 5c. Bio-oil and syngas reached 18 and 19 mass%, respectively. It has been shown that reducing the size of the particles to below 2 mm can improve heat transfer and raise the overall output of bio-oil [43].

FTIR analysis of bio-oil and biochar

Figure 6 explains the IR spectra of wood residue bio-oil fractions for different particle sizes. For particle sizes of 1, 2, and 3 cm, the results were very similar as appeared in Fig. 6a, b, and c, respectively. Samples indicate the existence of acid/methanol (3280 cm^{-1}), amide (1635 cm^{-1}), ketones (1563 cm^{-1}), and phenol (1060–1279 cm^{-1}) functional groups clearly [44–48]. The majority of the peaks seen in biochars observed in the spectra of FTIR analysis were common for different particle sizes, with notable exceptions as shown in Fig. 7. For particle size of 1 cm as shown in Fig. 7a, it is detected that the presence peak at 3490 cm^{-1} corresponds to OH stretching bond which in turn confirms the presence of hydroxyl and carboxyl functional groups. This peak disappeared in pyrolysis of larger particle size as shown in Fig. 7b, and c due to lower heat transfer ability. Also, alkynes (C≡C) and nitriles (C≡N) with triple bonds

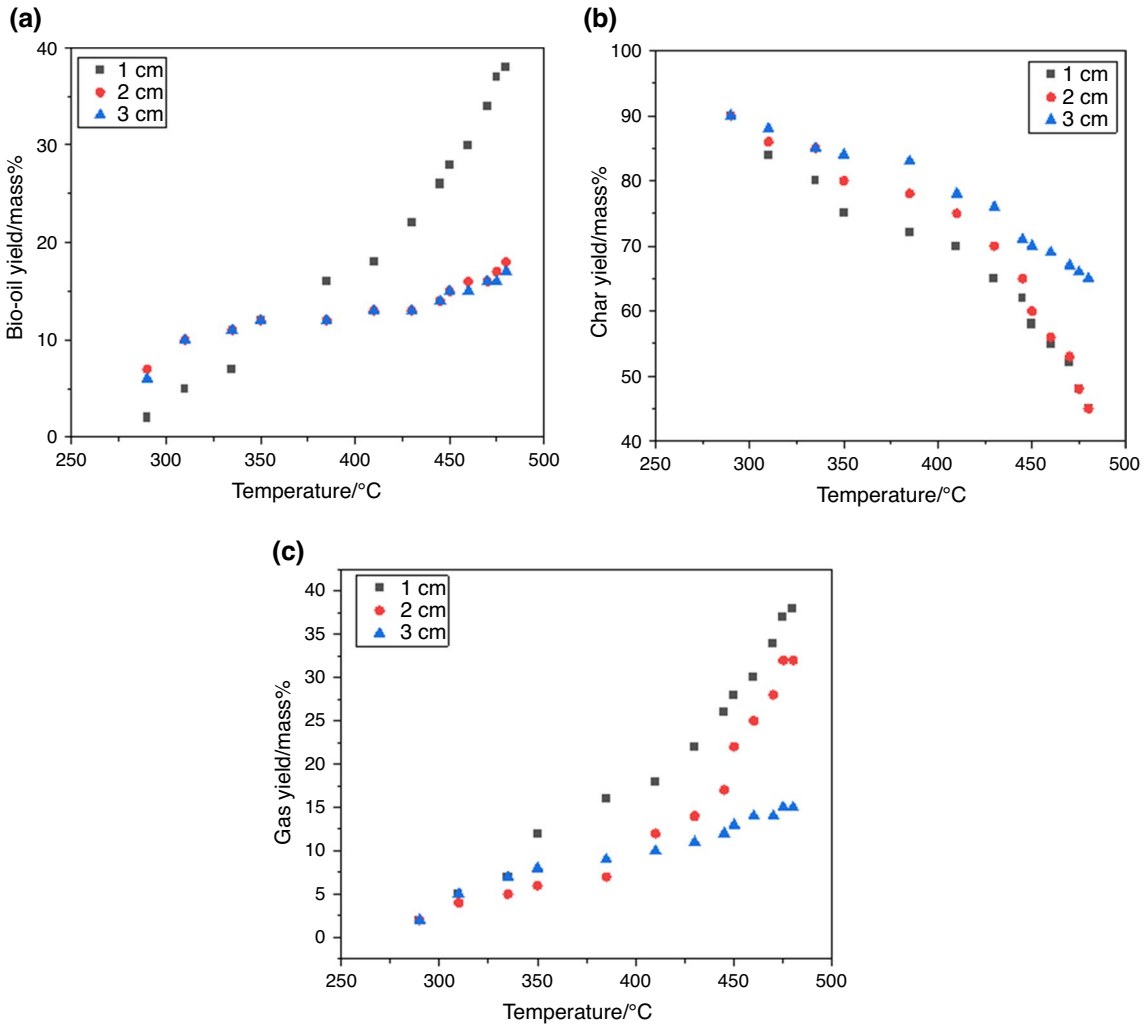


Fig. 4 Pyrolysis temperature influence on bio-oil, char, and gas yields

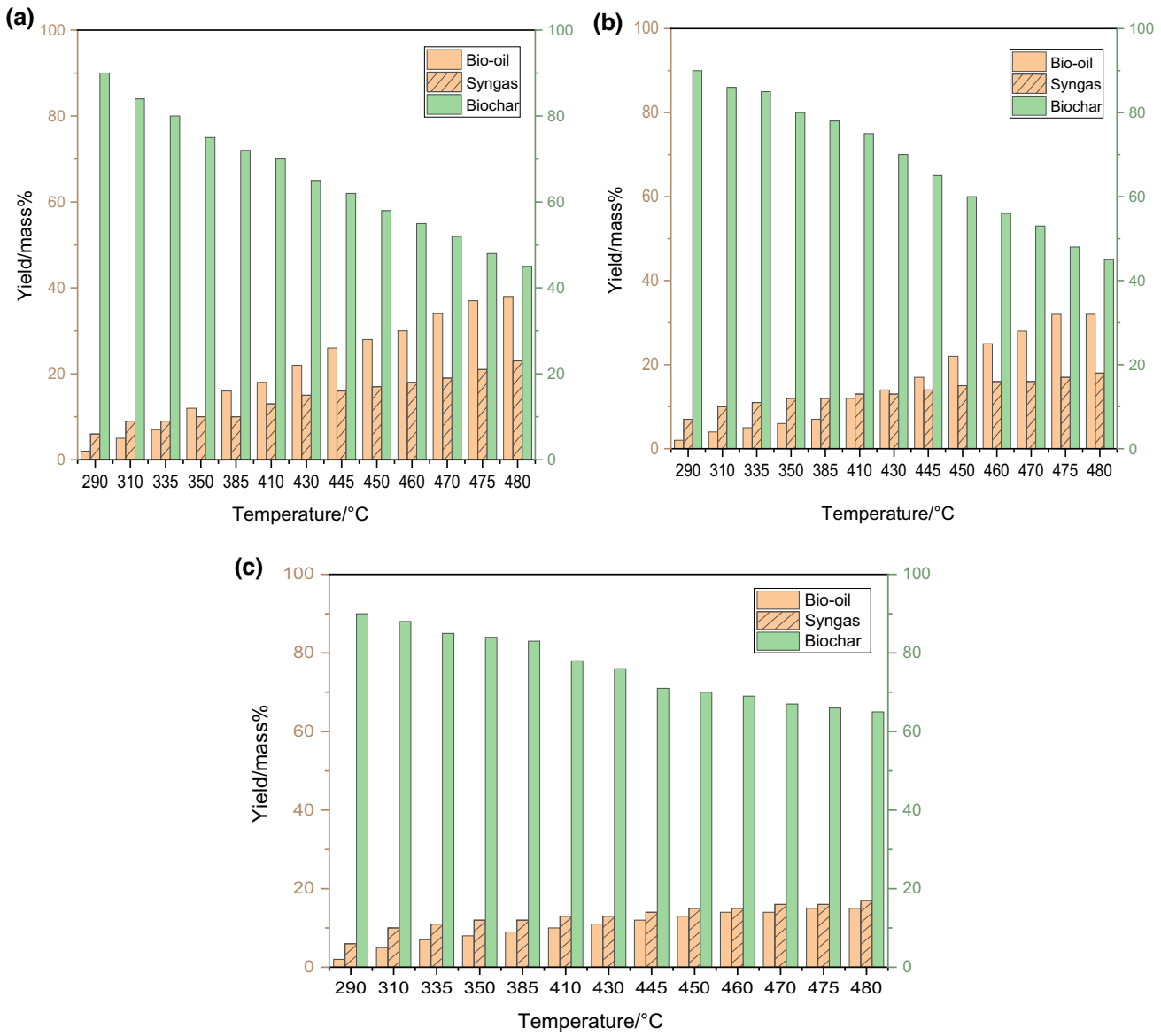


Fig. 5 Particle size influence on bio-oil, char, and gas yield **a** 1 cm **b** 2 cm **c** 3 cm

can be found in ranges between 2400 and 2100 cm^{-1}. The ranges from 1690 to 1570 cm^{-1} contain the double bond peak values for aromatic chains. The hydrogen assemblies are located outside the plane of the C-H bonds of the aromatic ring and have wavelengths between 850 and 750 cm^{-1}, while the angular deformations in the plane of the C-H bonds of the aromatic ring are in the angular range between 1172 cm^{-1} [49, 50].

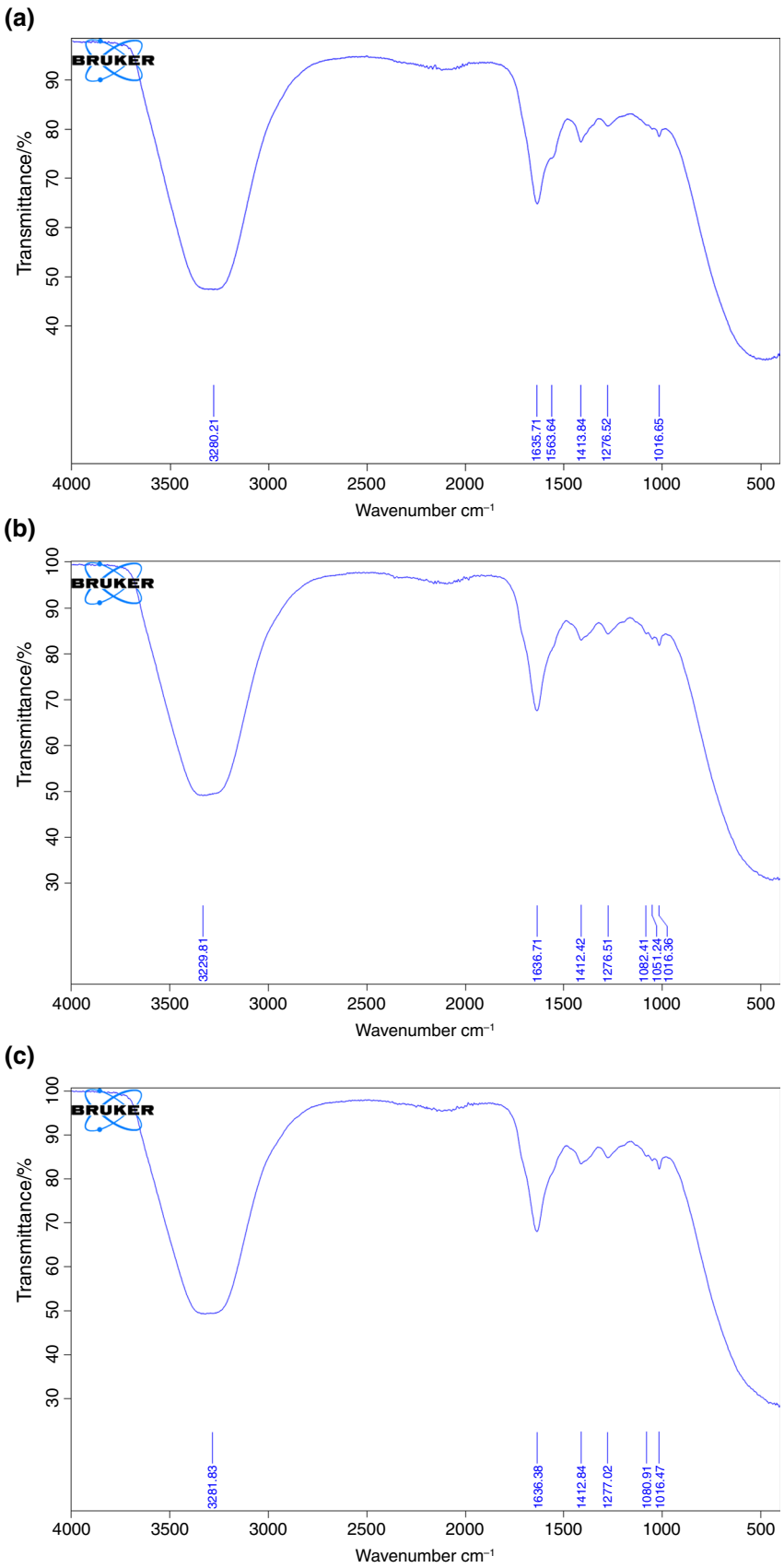


Fig. 6 FTIR spectra of bio-oil **a** 1 cm, **b** 2 cm, and **c** 3 cm

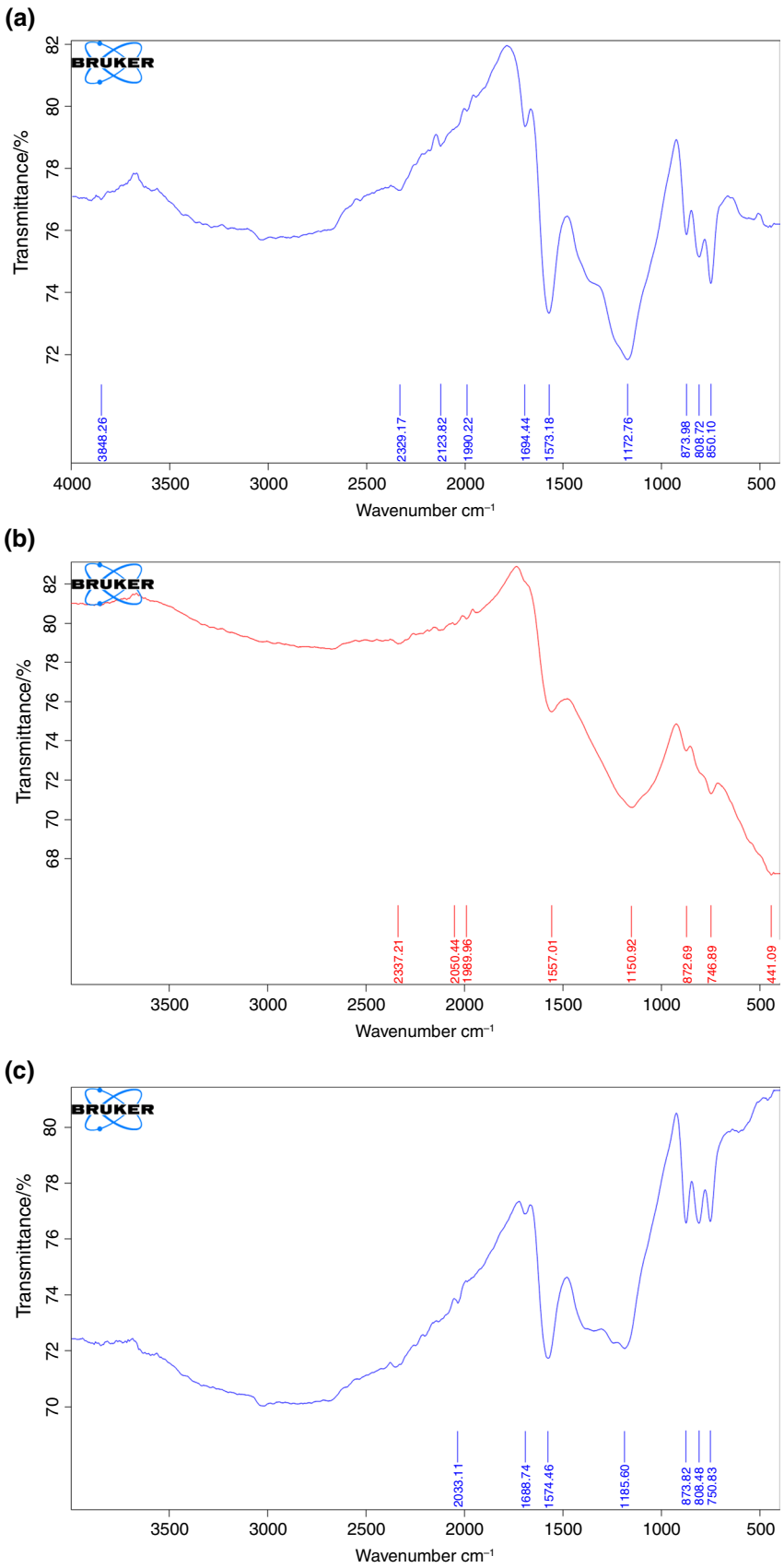


Fig. 7 FTIR spectra of bio-char **a** 1 cm, **b** 2 cm, and **c** 3 cm

Physicochemical properties of bio-oil

Table 2 displays the mass composition of the 23 basic chemical components that were identified by gas chromatography (GC) based on calibrations established using the relevant standards. The 23 compounds' combined mass contents ranged from 0.277 to 16.10 mass%, demonstrating a wide range in the chemical composition of bio-oil. Results indicate that the bio-oil contains phenolics (54.03%), acid (3.54%), alcohols (2.63%), aldehyde and ketones (1.9%), and other aromatic compounds. The pyrolysis oils were discovered to be chemically heterogeneous and are an excellent supplier of chemical raw materials in addition to being used as fuel.

Pyrolytic gas composition

Gaseous byproducts with compositions (mol) of 46.6% CO, 34.8% CO_2, 6.7% H_2, and 11.9% CH_4 are produced during the pyrolysis of wood residues at 450 °C. The HHV quantity of pyrolytic gas was determined to be 8.437 MJ kg^{-1} with the raw gaseous product, and this value is 17 MJ kg^{-1} excluding the composition of carbon dioxide, depending on the content of the current gaseous products. Through combustion, this pyrolytic gas can be employed to provide process heat. In the production of liquid fuel, hydrogen and carbon monoxide (syngas) can be utilized.

Surface morphology and composition of the biochar

Figure 8 shows the FE-SEM image of the produced char at a particle size of 1 cm, which illustrates the particle shape morphology. When compared to biochars at higher heating temperatures, it was found that the surface at a temperature of 300 °C is relatively flat; only a few shallow pores can be visible from the surface. The release of volatiles through the decomposition process adds to the creation of pores; this was probably caused by the insufficient breakdown of organic elements [51].

Also, for higher temperatures, the images indicated that the generated biochar contained irregularly spaced holes and fissures of varying intensities. This also was attributed to the enhanced rate of volatiles' decomposition and removal at higher pyrolysis temperatures, which also improved the biochar's surface roughness, surface area, active sites, cracks, and pore sizes [52]. The variation in carbon content of the biochar with temperature was examined by the EDX, and the results are presented in Table 3. For a temperature of 300 °C, the elemental mass of carbon was 75.35%. The carbon content has significantly increased by increasing heating temperature and reached 84.34% and 87.02% for 400 °C, and 450 °C, respectively. Results showed that raising the pyrolysis temperature increased organic volatilization in addition to high carbonization [53] (Table 4).

Simulation results and model validation

The simulation results versus the experimental results are shown in Fig. 9. The reduction in particle size enhanced the rate of mass transfer of volatile matter from the biomass which is reflected in the enhanced production of bio-oil and biogas. The simulation failed to detect this variation due to a change in mass transfer rate per unit area using the current modeling technique. However, the simulation served as a starting point for determining the best conditions for the production of either of the pyrolysis products. Gibbs free energy minimization approach is only dependent on the change in the composition of the system at constant temperature, pressure, and inlet composition. Therefore, it is not possible to model the effect of changing the biomass particle size on the pyrolysis products since the model presented in this study is only a function of pressure, temperature, and composition. The results fit well with the experimental data for the 3 cm wood residue. The highest difference in results is observed at the low-temperature range (i.e., 290 °C – 350 °C). The results from the proposed model agreeing well with the 3 cm wood residue can be justified by the fact that equilibrium is attained at fast reaction rates and long residence time. The reaction rate increases as the particle size of the biomass decreases as a result of the larger surface. On the other hand, the residence time of the biomass decreases considerably at smaller particle sizes due to the rapid consumption of the solid biomass resulting in a higher production of gas and oil. Therefore, the equilibrium model best fitted the 3 cm wood residue case at higher temperatures due to the fast reaction rate accompanied with the long residence time of the pyrolyzed biomass [26, 54].

Table 3 GC–MS analysis of bio-oil

Compound Name	Molecular Formula	Peak Area /%
Octanenitrile	$C_8H_{15}N$	2.5249
Ethanone, 1-(1H-pyrazol-4-yl)-	$C_5H_6N_2O$	5.8039
Oxalic acid, isobutyl pentadecyl ester	$C_{21}H_{40}O_4$	3.5472
Cyclobutanone, 2-methyl-2-oxiranyl-	$C_7H_{10}O_2$	1.7094
2-Cyclopenten-1-one, 3-methyl-	C_6H_8O	3.3891
2-Furancarboxaldehyde, 5-methyl-	$C_6H_6O_2$	1.9028
Phenol	C_6H_6O	16.0918
Phenol, 2-methoxy-	$C_{10}H_{12}O_2$	13.3529
p-Cresol	C_7H_8O	10.1343
Creosol	$C_8H_{10}O_2$	11.3993
2-Cyclopenten-1-one, 2,3,4,5-tetramethyl-	$C_9H_{14}O$	2.2485
Silane, 1,3-butadiynyltrimethyl-	$C_{10}H_{20}OSi$	1.4819
Phenol, 4-ethyl-2-methoxy-	$C_9H_{12}O_2$	3.0105
3-Butenoic acid, 2,2-dimethyl-	$C_6H_{10}O_2$	3.9199
3,5-Dimethoxybenzyl alcohol	$C_9H_{12}O_4$	2.6291
Vanillin	$C_8H_8O_3$	0.4643
2-Propanone, 1-(4-hydroxy-3-methoxyphenyl)-	$C_{10}H_{12}O_3$	6.2448
2(3H)-Naphthalenone, 4,4a,5,6,7,8-hexahydro-1-methoxy-	$C_{11}H_{16}O_2$	1.3776
2,5-Cyclohexadiene-1,4-dione, 3-hydroxy-2-methyl-5-(1-methylethyl)-	$C_{10}H_{12}O_3$	0.2764
1-(1-Hydroxybutyl)-2,5-dimethoxybenzene	$C_{12}H_{18}O_3$	0.4494
l-(+)-Ascorbic acid 2,6-dihexadecanoate	$C_{38}H_{68}O_8$	0.6403
2-(Acetoxymethyl)-3-(methoxycarbonyl)biphenylene	$C_{17}H_{14}O_4$	6.9132
Pyrido[2,3-d]pyrimidine, 4-phenyl-	$C_{13}H_9N_3$	0.4103

Table 4 EDX elemental composition by mass percentage

Temperature	300 °C	400 °C	450 °C
Element	mass %		
Carbon (C)	75.35	84.34	87.02
Oxygen (O)	24.65	15.66	12.98
Total	100	100	100

Conclusions

Biomass waste pyrolysis can act as a promising energy source. The Aspen Plus simulation model was built using the experimental settings as input, and the simulation results were then compared to the outcomes of the experiment. The experimental system was employed at temperatures ranging between 280 and 490 °C. In this study, experiments on a reactor for wood residue biomass pyrolysis were carried out at various temperatures (290–480 °C). To validate the experimental work, a model of the pyrolysis processes for wood residues was employed using Aspen Plus software. The results showed that fixed carbon content in wood residues reached 12.68% with higher amounts of O and C. Also, increasing the pyrolysis temperature from 290 to 480 °C has significantly raised the bio-oil yield from 2 to 38%. For particle size 1 cm, the results showed a superior conversion for the biomass residues. Moreover, the results indicated that the bio-oil contains phenolics (54.03%), acid (3.54%), alcohols (2.63%), aldehyde and ketones (1.9%), and other aromatic compounds. Simulation results fit well with the experimental data for the 3 cm wood residue. The highest difference in results is observed at the low-temperature range (i.e., 290–350°C). A simulation model based on the fluidized bed reactor available in the more recent versions of Aspen Plus should tackle the limitations in the current model. The fluidized bed model enables introducing the complex interactions between heat transfer, mass transfer, hydrodynamics, and chemical kinetics which is believed to be highly promising in simulating the pyrolysis process.

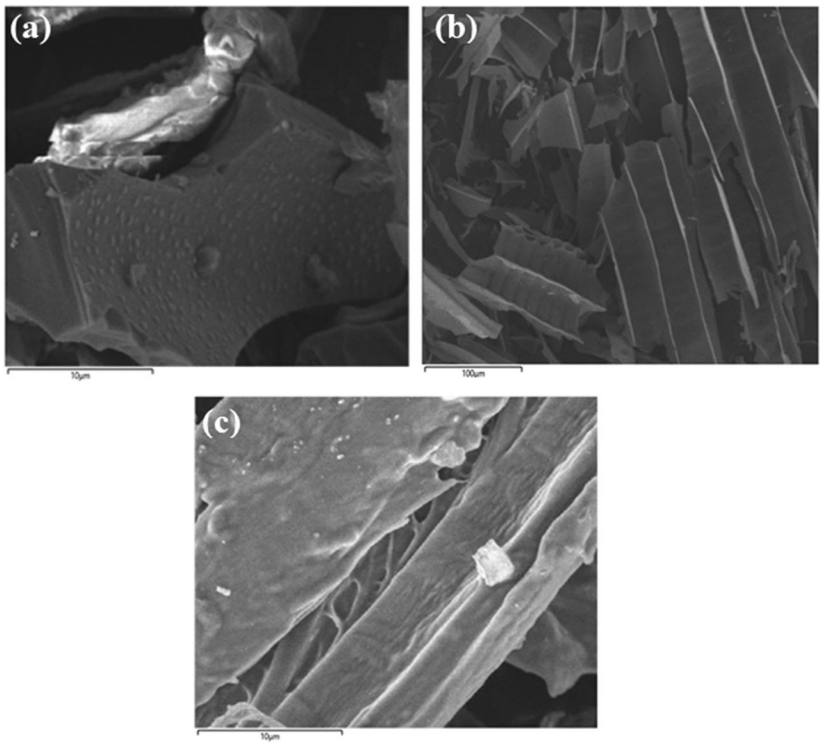


Fig. 8 FE-SEM images of biochar **a** 300 °C, **b** 400 °C, and **c** 500 °C

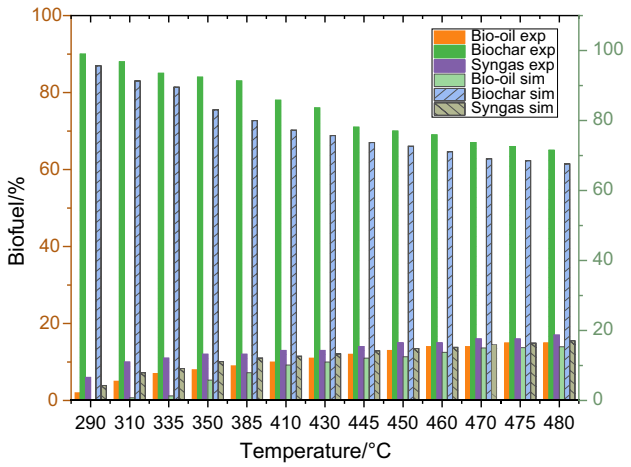


Fig. 9 Simulation results versus the experimental results of the 3 cm strips at a temperature range of 290–480 °C

Acknowledgements The researchers would like to acknowledge the assistance provided by the South African National Energy Development Institute (SANEDI) for funding the project. This project has received funding from the European Union's Horizon 2020 Research and Innovation Programme under Grant Agreement 963530.

Author contributions Conceptualization was performed by YE and KF; methodology by YE, MB, and AM; software by AM and MG; formal analysis by YEMB; investigation by FA and TM; resources by FA and TM; data curation by YE, KF, MB, AM, MG, FA, and TM; writing—original draft preparation—by YE, KF, MB, AM, MG, FA, and TM; writing—review and editing—by YE, KF, MB, AM, MG, FA, and TM; visualization by YE, KF, MB, AM, MG, FA, and TM; supervision by YE, KF, MB, AM, MG, FA, and TM; project administration by FA and TM; funding acquisition by FA and TM. All authors have read and agreed to the published version of the manuscript.

Funding Open access funding provided by University of the Witwatersrand.

Open Access This article is licensed under a Creative Commons Attribution 4.0 International License, which permits use, sharing, adaptation, distribution and reproduction in any medium or format, as long as you give appropriate credit to the original author(s) and the source, provide a link to the Creative Commons licence, and indicate if changes were made. The images or other third party material in this article are included in the article's Creative Commons licence, unless indicated otherwise in a credit line to the material. If material is not included in the article's Creative Commons licence and your intended use is not permitted by statutory regulation or exceeds the permitted use, you will need to obtain permission directly from the copyright holder. To view a copy of this licence, visit http://creativecommons.org/licenses/by/4.0/.

References

1. Hu X, Gholizadeh M. Biomass pyrolysis: a review of the process development and challenges from initial researches up to the commercialisation stage. J Energy Chem. 2019;39:109–43. https://doi.org/10.1016/j.jechem.2019.01.024.
2. Hasan MM, Rasul MG, Jahirul MI, Khan MMK. Modeling and process simulation of waste macadamia nutshell pyrolysis using Aspen Plus software. Energy Rep. 2022;8:429–37. https://doi.org/10.1016/j.egyr.2022.10.323.

3. Konur O. Crude oils: a scientometric review of the research. Petrodiesel Fuels. 2021;3:837–58.
4. Kuppusamy S, Maddela NR, Megharaj M, Venkateswarlu K. An overview of total petroleum hydrocarbons. Total Pet Hydrocarb Environ Fate Toxic Remed. 2020. https://doi.org/10.1007/978-3-030-24035-6_1.
5. Jitumoni B, Dixit SA, Pradeep PR, Ravindra K, Das SK, Christopher J, et al. Study of thermal cracking kinetics and co-processing of biocrude in thermal residual upgradation unit for converting 'waste to energy.' J Therm Anal Calorim. 2023;148:3439–56. https://doi.org/10.1007/s10973-023-11941-8.
6. Mohd Mokhta Z, Ong MY, Salman B, Nomanbhay S, Salleh SF, Chew KW, et al. Simulation studies on microwave-assisted pyrolysis of biomass for bioenergy production with special attention on waveguide number and location. Energy. 2020;190:116474. https://doi.org/10.1016/j.energy.2019.116474.
7. Zhao H, Jin L, Wang M, Wei B, Hu H. Integrated process of coal pyrolysis with catalytic reforming of simulated coal gas for improving tar yield. Fuel. 2019;255:115797. https://doi.org/10.1016/j.fuel.2019.115797.
8. Elhenawy Y, Moustafa GH, Attia AM, Mansi AE, Majozi T, Bassyouni M. Performance enhancement of a hybrid multi effect evaporation/membrane distillation system driven by solar energy for desalination.". J Environ Chem Eng. 2022;10(6):108855. https://doi.org/10.1016/j.jece.2022.108855.
9. Ben Abdallah A, Ben Hassen Trabelsi A, Navarro MV, Veses A, García T, Mihoubi D. Pyrolysis of tea and coffee wastes: effect of physicochemical properties on kinetic and thermodynamic characteristics. J Therm Anal Calorim. 2023;148:2501–15. https://doi.org/10.1007/s10973-022-11878-4.
10. Hasan MM, Rasul MG, Khan MMK, Ashwath N, Jahirul MI. Energy recovery from municipal solid waste using pyrolysis technology: a review on current status and developments. Renew Sustain Energy Rev. 2021;145:111073. https://doi.org/10.1016/j.rser.2021.111073.
11. Elminshawy NAS, Gadalla MA, Bassyouni M, El-Nahhas K, Elminshawy A, Elhenawy Y. A novel concentrated photovoltaic-driven membrane distillation hybrid system for the simultaneous production of electricity and potable water. Renew Energy. 2020;162:802–17. https://doi.org/10.1016/j.renene.2020.08.041.
12. Rashedi A, Khanam T, Jonkman M. On reduced consumption of fossil fuels in 2020 and its consequences in global environment and exergy demand. Energies. 2020;22:6048.
13. Faraji M, Saidi M. Hydrogen-rich syngas production via integrated configuration of pyrolysis and air gasification processes of various algal biomass: process simulation and evaluation using Aspen Plus software. Int J Hydrogen Energy. 2021;46:18844–56. https://doi.org/10.1016/j.ijhydene.2021.03.047.
14. Sait HH, Hussain A, Bassyouni M, Ali I, Kanthasamy R, Ayodele BV, et al. Hydrogen-rich syngas and biochar production by non-catalytic valorization of date palm seeds. Energies. 2022;15:1–13.
15. Tezer Ö, Karabağ N, Öngen A, Çolpan CÖ, Ayol A. Biomass gasification for sustainable energy production: a review. Int J Hydrogen Energy. 2022;47:15419–33.
16. Bassyouni M, Ul Hasan SW, Abdel-Aziz MH, Abdel-Hamid SMS, Naveed S, Hussain A, et al. Date palm waste gasification in downdraft gasifier and simulation using ASPEN HYSYS. Energy Convers Manag. 2014;88:693–9. https://doi.org/10.1016/j.enconman.2014.08.061.
17. Mensah RA, Jiang L, Renner JS, Xu Q. Characterisation of the fire behaviour of wood: from pyrolysis to fire retardant mechanisms. J Therm Anal Calorim. 2023;148:1407–22. https://doi.org/10.1007/s10973-022-11442-0.
18. Mlonka-Mędrala A, Evangelopoulos P, Sieradzka M, Zajemska M, Magdziarz A. Pyrolysis of agricultural waste biomass towards production of gas fuel and high-quality char: experimental and numerical investigations. Fuel. 2021;296:120611.
19. Kaczor Z, Buliński Z, Werle S. Modelling approaches to waste biomass pyrolysis: a review. Renew Energy. 2020;159:427–43.
20. Silveira EA, Santanna MS, Barbosa Souto NP, Lamas GC, Galvão LGO, Luz SM, et al. Urban lignocellulosic waste as biofuel: thermal improvement and torrefaction kinetics. J Therm Anal Calorim. 2023;148:197–212. https://doi.org/10.1007/s10973-022-11515-0.
21. Uddin MN, Techato K, Taweekun J, Rahman MM, Rasul MG, Mahlia TMI, et al. An overview of recent developments in biomass pyrolysis technologies. Energies. 2018;11(11):3115.
22. Elsawy K, Elhenawy Y, Abdelmotalip A, Ibrahim IA. Biogas production by anaerobic digestion of cow dung using floating type fermenter. J Environ Treat Tech. 2021;9:446–51.
23. Marrakchi F, Wei M, Cao B, Yuan C, Chen H, Wang S. Copyrolysis of microalga Chlorella sp. and alkali lignin with potassium carbonate impregnation for synergistic Bisphenol A plasticizer adsorption. Int J Biol Macromol. 2023;228:808–15. https://doi.org/10.1016/j.ijbiomac.2022.12.207.
24. Vieira FR, Romero Luna CM, Arce GLAF, Ávila I. Optimization of slow pyrolysis process parameters using a fixed bed reactor for biochar yield from rice husk. Biomass Bioenergy. 2020;132:105412.
25. Jiang D, Li H, Cheng X, Abomohra A, Hu Y, Babadi AA, et al. Chemical process of multiphase system in lignin-biochar co-pyrolysis for enhanced phenol recovery. Fuel Process Technol. 2023;250:107882. https://doi.org/10.1016/j.fuproc.2023.107882.
26. Shahbaz M, AlNouss A, Parthasarathy P, Abdelaal AH, Mackey H, McKay G, Al-Ansari T. Investigation of biomass components on the slow pyrolysis products yield using Aspen Plus for techno-economic analysis. Biomass Conversion and Biorefinery. 2022;12:669–81. https://doi.org/10.1007/s13399-020-01040-1.
27. Han D, Yang X, Li R, Wu Y. Environmental impact comparison of typical and resource-efficient biomass fast pyrolysis systems based on LCA and Aspen Plus simulation. J Clean Prod. 2019;231:254–67. https://doi.org/10.1016/j.jclepro.2019.05.094.
28. Usman MA, Fagoroye OK, Ajayi TO, Kehinde AJ. ASPEN plus simulation of liquid–liquid equilibria data for the extraction of aromatics from waste tyre pyrolysis gasoline using organic and deep eutectic solvents: a comparative study. Appl Petrochemical Res. 2021;11:113–22. https://doi.org/10.1007/s13203-020-00262-8.
29. Liu Y, Yang X, Zhang J, Zhu Z. Process simulation of preparing biochar by biomass pyrolysis via aspen plus and its economic evaluation. Waste Biomass Valorization. 2022;13:2609–22.
30. AlNouss A, Parthasarathy P, Mackey HR, Al-Ansari T, McKay G. Pyrolysis study of different fruit wastes using an Aspen Plus model. Front Sustain Food Syst. 2021;5:604001.
31. Kabir MJ, Chowdhury AA, Rasul MG. Pyrolysis of municipal green waste: a modelling, simulation and experimental analysis. Energies. 2015;8(8):7522–41.
32. Salehi E, Abedi J, Harding T. Bio-oil from sawdust: pyrolysis of sawdust in a fixed-bed system. Energy Fuels. 2009;23:3767–72.
33. Ahmed A, Bakar MSA, Sukri RS, Hussain M, Farooq A, Moogi S, Park YK. Sawdust pyrolysis from the furniture industry in an auger pyrolysis reactor system for biochar and bio-oil production. Energy Convers Manage. 2020;226: 113502.
34. Nam H, Capareda S. Experimental investigation of torrefaction of two agricultural wastes of different composition using RSM (response surface methodology). Energy. 2015;91:507–16. https://doi.org/10.1016/j.energy.2015.08.064.
35. Park J, Lee Y, Ryu C, Park YK. Slow pyrolysis of rice straw: analysis of products properties, carbon and energy yields. Bioresour Technol. 2014;155:63–70. https://doi.org/10.1016/j.biortech.2013.12.084.

36. Testa L, Chiaramonti D, Prussi M, Bensaid S. Challenges and opportunities of process modelling renewable advanced fuels. Biomass Convers Biorefinery. 2022;12:1–36. https://doi.org/10.1007/s13399-022-03057-0.
37. Peters JF, Iribarren D, Dufour J Predictive pyrolysis process modelling in Aspen Plus. In: 21st Eur biomass conf exhib, pp 923–927. 2013
38. Ke Y, Cui S, Fu Q, Hough R, Zhang Z, Li YF. Effects of pyrolysis temperature and aging treatment on the adsorption of Cd2+ and Zn2+ by coffee grounds biochar. Chemosphere. 2022;296:134051. https://doi.org/10.1016/j.chemosphere.2022.134051.
39. Hoang AT, Ong HC, Fattah IMR, Chong CT, Cheng CK, Sakthivel R, et al. Progress on the lignocellulosic biomass pyrolysis for biofuel production toward environmental sustainability. Fuel Process Technol. 2021;223:106997. https://doi.org/10.1016/j.fuproc.2021.106997.
40. Shen Q, Liaw SB, Costa M, Wu H. Rapid pyrolysis of pulverized biomass at a high temperature: the effect of particle size on char yield, retentions of alkali and alkaline earth metallic species, and char particle shape. Energy Fuels. 2020;34:7140–8.
41. Islam MN, Islam MN, Beg MRA, Islam MR. Pyrolytic oil from fixed bed pyrolysis of municipal solid waste and its characterization. Renew Energy. 2005;30:413–20.
42. Anandaram H, Srivastava BK, Vijayakumar B, Madhu P, Depoures MV, Patil PP, et al. Co-pyrolysis characteristics and synergistic interaction of waste polyethylene terephthalate and woody biomass towards bio-oil production. J Chem. 2022;2022:1–9.
43. Bridgewater AV. Biomass fast pyrolysis. Therm Sci. 2004;8:21–50.
44. Abnisa F, Arami-Niya A, Daud WMAW, Sahu JN. Characterization of bio-oil and bio-char from pyrolysis of palm oil wastes. Bioenergy Res. 2013;6:830–40.
45. Wang Y, Han Y, Hu W, Fu D, Wang G. Analytical strategies for chemical characterization of bio-oil. J Sep Sci. 2020;43:360–71.
46. Saraçoğlu E, Uzun BB, Apaydın-Varol E. Upgrading of fast pyrolysis bio-oil over Fe modified ZSM-5 catalyst to enhance the formation of phenolic compounds. Int J Hydrogen Energy. 2017;42:21476–86.
47. Xiu S, Shahbazi A, Shirley V, Cheng D. Hydrothermal pyrolysis of swine manure to bio-oil: Effects of operating parameters on products yield and characterization of bio-oil. J Anal Appl Pyrolysis. 2010;88:73–9. https://doi.org/10.1016/j.jaap.2010.02.011.
48. Sugumaran V, Prakash S, Ramu E, Arora AK, Bansal V, Kagdiyal V, et al. Detailed characterization of bio-oil from pyrolysis of non-edible seed-cakes by Fourier Transform Infrared Spectroscopy (FTIR) and gas chromatography mass spectrometry (GC–MS) techniques. J Chromatogr B Anal Technol Biomed Life Sci. 2017;1058:47–56. https://doi.org/10.1016/j.jchromb.2017.05.014.
49. Rodriguez JA, Lustosa Filho JF, Melo LCA, de Assis IR, de Oliveira TS. Influence of pyrolysis temperature and feedstock on the properties of biochars produced from agricultural and industrial wastes. J Anal Appl Pyrolysis. 2020;149:104839. https://doi.org/10.1016/j.jaap.2020.104839.
50. Sahoo K, Kumar A, Chakraborty JP. A comparative study on valuable products: bio-oil, biochar, non-condensable gases from pyrolysis of agricultural residues. J Mater Cycles Waste Manag. 2021;23:186–204. https://doi.org/10.1007/s10163-020-01114-2.
51. Pütün E, Pyrolysis A sustainable way from biomass to biofuels and biochar. Biochar. 2016 239
52. Ahmed A, Abu Bakar MS, Sukri RS, Hussain M, Farooq A, Moogi S, et al. Sawdust pyrolysis from the furniture industry in an auger pyrolysis reactor system for biochar and bio-oil production. Energy Convers Manag. 2020;226:113502. https://doi.org/10.1016/j.enconman.2020.113502.
53. Waqas M, Aburiazaiza AS, Miandad R, Rehan M, Barakat MA, Nizami AS. Development of biochar as fuel and catalyst in energy recovery technologies. J Clean Prod. 2018;188:477–88. https://doi.org/10.1016/j.jclepro.2018.04.017.
54. Chen Z, Zhang X, Che L, Peng H, Zhu S, Yang F, et al. Effect of volatile reactions on oil production and composition in thermal and catalytic pyrolysis of polyethylene. Fuel. 2020;271:117308. https://doi.org/10.1016/j.fuel.2020.117308.

Publisher's Note Springer Nature remains neutral with regard to jurisdictional claims in published maps and institutional affiliations.